Additive Manufacturing 24 (2018) 224–231

Contents lists available at ScienceDirect

Additive Manufacturing

journal homepage: www.elsevier.com/locate/addma

# Measurement and modeling of filament temperature distribution in the standoff gap between nozzle and bed in polymer-based additive manufacturing

Hardikkumar Prajapati, Darshan Ravoori, Ankur Jain*

*Mechanical and Aerospace Engineering Department, University of Texas at Arlington, Arlington, TX, USA*

ARTICLE INFO

*Keywords:*
Additive manufacturing
Polymer extrusion
Infrared thermography
Heat transfer analysis

ABSTRACT

Dispensing of a polymer filament above its glass transition temperature is a critical step in several polymer-based additive manufacturing techniques. While the nozzle assembly heats up the filament prior to dispense, it is important to minimize cooling down of the filament in the standoff distance between the nozzle tip and bed. While heat transfer processes within the nozzle assembly, such as filament melting, and on the bed, such as thermally-driven filament-to-filament adhesion, have been well studied, there is a lack of work on heat transfer in the filament in the standoff region. This paper presents infrared thermography based measurement of temperature distribution in the filament in the standoff region, and an analytical model for heat transfer in this region. The analytical model, based on a balance between thermal advection and convective/radiative heat loss predicts an exponentially decaying temperature distribution, the nature of which is governed by the characteristic length, a parameter that combines multiple process parameters such as mass flowrate, filament diameter, heat capacity and cooling conditions. Experimental data in a wide range of process parameters are found to be in very good agreement with the analytical model. The thermal design space for ensuring minimal temperature drop in the standoff region is explored based on the analytical model. Experimental data and theoretical modeling presented here improve our fundamental understanding of heat transfer in polymer additive manufacturing, and may contribute towards design tools for thermal optimization of these processes.

## 1. Introduction

Fused filament fabrication [1–4] is a broad class of additive manufacturing (AM) processes based on heating up of a thermoplastic polymer wire to above its glass transition temperature, followed by extrusion and selective dispensing of the filament on a bed, where adjacent filaments bond with each other in order to form the eventual part. Compared to metal based AM, polymer based additive manufacturing is more easily accessible due to relatively lower cost, and therefore has been widely used for multiple applications [5–7]. However, there are several challenges associated with having to ensure good bonding between adjacent filaments for acceptable physical properties of the built part [8–10].

Multiple heat transfer processes occur during polymer additive manufacturing and impact the quality of the built part [8–14]. A comprehensive understanding of thermal effects during polymer AM is critical for optimizing the properties of the built part. Fig. 1(a) shows a schematic of this process, which can be divided into three distinct regions, each with a set of key heat transfer processes – within the nozzle assembly prior to dispense, during filament travel from nozzle tip to bed, and on the bed. Important heat transfer processes in the nozzle assembly prior to dispensing include heating up of the polymer wire in the barrel and extrusion of the softened wire through the nozzle tip. Once dispensed on the bed, heat transfer occurs from the filament to the bed, adjacent filaments and the surroundings [10,12,15]. The nature of these processes on the bed ultimately determines the extent of bonding between adjacent filaments, and therefore the overall quality of the part [10]. In addition to the nozzle assembly and the bed, Fig. 1(a) also shows a standoff region between the two that the filament travels through. Even though the stand-off distance is usually very short (lower than 1 mm), heat transfer in this region may be important to study as it determines the temperature of the filament reaching the bed. Process parameters must be chosen such that the filament does not significantly cool down between the nozzle tip and bed, so that the filament is delivered on the bed at a temperature close to the nozzle tip temperature.

* Corresponding author at: 500W First St, Rm 211, Arlington, TX, 76019, USA.
*E-mail address:* jaina@uta.edu (A. Jain).

https://doi.org/10.1016/j.addma.2018.09.030
Received 12 July 2018; Received in revised form 13 September 2018; Accepted 25 September 2018
Available online 26 September 2018

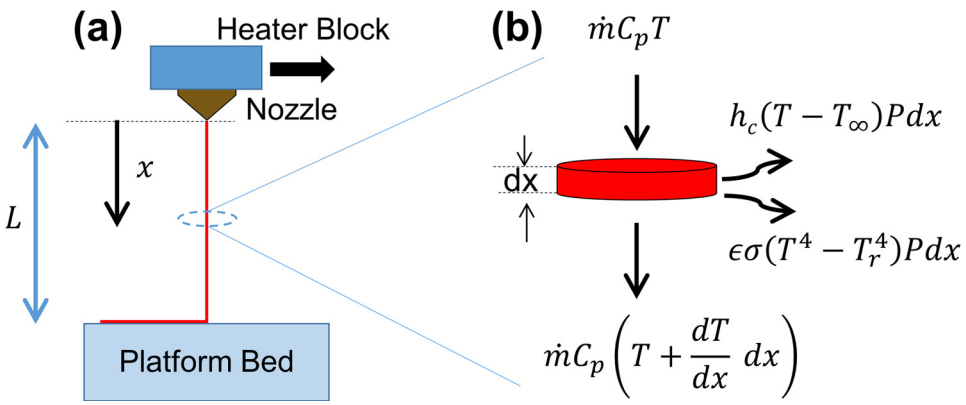


**Fig. 1.** (a) Schematic of a typical polymer extrusion process showing the standoff region between the nozzle tip and platform. Note that this schematic is not drawn to scale. The standoff region is significantly enlarged for clarity. (b) steady state energy balance in an infinitesimal element in the filament in the standoff region showing thermal advection, convection and radiation.

Significant research has been carried out on understanding heat transfer processes within the nozzle assembly and on the bed. Several papers have reported thermal modeling and measurements of processes in the nozzle assembly in which the polymer is melted and extruded through a nozzle [13,14,16]. Temperature has been measured through embedded thermocouples [14]. Theoretical modeling and finite-element simulations have been reported for characterizing heat transfer, fluid flow and polymer rheology in the barrel [17–19]. Heat transfer from the barrel walls to the polymer is a key challenge here due to poor thermal conductivity of the polymer [20]. Preheating the polymer wire prior to entering the barrel has been explored as a means to improve thermal performance [20]. Infrared thermometry has also been used for measuring the temperature field in the heater block prior to dispense [20]. Hydrodynamics, non-Newtonian flow, viscoelastic effects and material rheology have all been recognized as having significant impact on thermal performance within the nozzle, and have thus been studied in detail [16,21,22].

Significant amount of work has also been carried out for understanding heat transfer in the bed once the filament has been deposited [8–12]. Temperature distribution during the filament bonding process has been measured through infrared thermometry [23]. Relationships between the temperature field and quality of filament-to-filament bonding have been studied [10]. Theoretical modeling and numerical simulations of heat transfer within the filament, between filament and ambient, and between filament and bed have been carried out [15]. Numerical simulation of heat transfer between successive layers has also been reported [24]. It has been shown that print speed influences the rate at which the filament cools down after deposition, but not the extent of bonding between adjacent filaments [25]. Past research in this direction indicates that bed temperature and filament temperature as deposited on the platform both govern the bonding process on the bed after the filament has been deposited [10,24]. In particular, the filament temperature at the end of the standoff region provides the thermal initial condition from where the temperature of the filament evolves as heat is transferred from the newly deposited filament to adjacent filaments, bed and the ambient. This highlights the importance of studying heat transfer in the standoff region, and of understanding which experimental parameters influence the filament temperature at the end of the standoff region. It is important to design the dispense process and standoff distance in order to minimize temperature drop in the standoff region so that the filament is deposited at nearly the same temperature as the nozzle tip.

While heat transfer processes in the nozzle and on the bed are relatively well understood, relatively less work has been reported on modeling and measurements in the standoff distance between the nozzle tip and bed. Even though the standoff distance is very short, heat transfer in this region is very important to study, since cooling off of the filament during this process may severely reduce the filament temperature as it hits the bed, and therefore impact the quality of bonding. While nozzle temperature, stand-off distance and cooling conditions are all expected to play a key role in determining filament temperature distribution in the standoff region, an exact relationship between these parameters and the temperature distribution is not known. Clearly, there is a need for theoretical modeling of this process in order to develop accurate, predictive tools and for experimental validation through systematic measurements. Infrared thermography has been used in the past to measure the temperature profile of extruded polyethylene terephthalate (PET) microfibers from a die, but not for parameters typical for polymer AM [26]. The small value of the stand-off distance, small size of the filament and need for non-intrusive temperature measurement all present significant challenges in this direction.

This paper presents theoretical modeling and experimental measurement of temperature distribution in the polymer filament in the stand-off region between the nozzle and bed. Based on an assumption of thermal steady state, an ordinary differential equation for the temperature distribution is derived and solved. The resulting solution shows that the temperature distribution is governed by a single parameter $x_0$, which is named the characteristic length. Two distinct heat transfer regimes in the standoff region are identified based on the value of $x_0$ relative to the standoff length. Experimental measurement of temperature distribution in the filament between the nozzle and bed using infrared thermography is found to be in good agreement with the theoretical model in a wide variety of experimental conditions. The validated theoretical model is analyzed for understanding the parametric regimes that result in low temperature drop between the nozzle and bed. Heat transfer analysis and measurements presented in this work improve our fundamental understanding of polymer based additive manufacturing processes, and may result in practical design tools for improving and optimizing these processes.

Section 2 describes the experimental set up and measurements carried out. Section 3 presents the analytical heat transfer model. Key theoretical and experimental results are discussed in Section 4, followed by conclusions in Section 5.

## 2. Experiments

Experiments are carried out to quantitatively measure the temperature distribution in the filament in the standoff region after being extruded from the nozzle tip through infrared thermography. A custom-built platform for filament dispensing with controlled process parameters and optical access for infrared thermography is designed and built for this purpose.

### 2.1. Extruder arrangement

Commercially available polymer AM platforms do not provide sufficient flexibility to vary process parameters of interest in this work and also do not offer good optical access to the standoff region. As a result, an in-house polymer extruder and dispenser setup is designed and

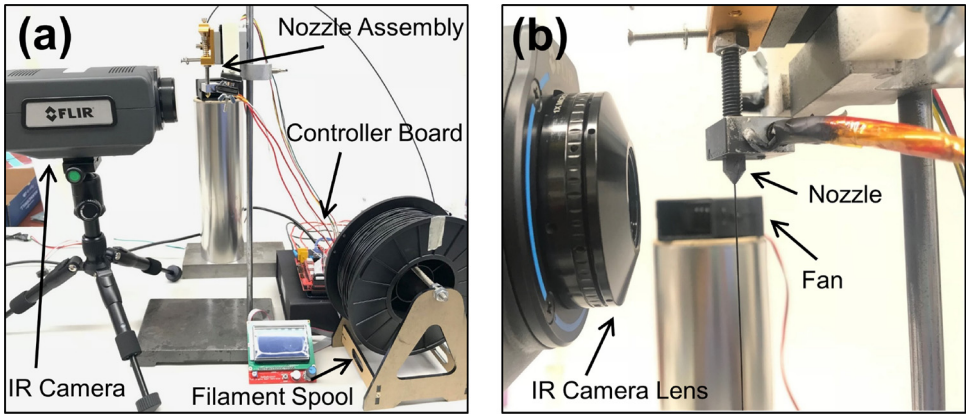


**Fig. 2.** (a) Picture of the experimental setup showing the custom-built extruder assembly and infrared camera. (b) Zoom-in picture showing the nozzle tip and extruding filament.

assembled to facilitate careful variation and measurement of various parameters such as filament speed, nozzle diameter, etc. while also offering optical access for an infrared camera to measure temperature variation along the length of the extruded material. Fig. 2(a) presents a schematic of the experimental setup, showing the key components, including a control circuit, stepper motor, and heater-nozzle assembly. Stepper motor speed and heater block temperature are controlled by an Arduino Mega 2560 circuit board running a RAMPS A4988 stepper motor driver using Repetier-Host V2.0.5 software. The filament is fed through a NEMA 17 stepper motor to the Aluminum heater block. Calibration for the stepper motor is entered in the motor firmware for each nozzle diameter and verified through test runs. 1.75 mm diameter Acrylonitrile butadiene styrene (ABS) Black filament material from Makerbot is used in all experiments. Fig. 2(b) shows a zoom-in image of the active area in the experiment, including the polymer dispensing nozzle, IR camera lens and a cooling fan in the background used in some of the experiments.

There is no print bed under the filament being dispensed. This is justified because the print bed temperature is not expected to have a significant impact of filament temperature distribution in the standoff region due to the large value of the Peclet number [27], which is the ratio of thermal advection downstream to thermal diffusion upstream. This is discussed further in Section 3. Separate experiments are carried out in which temperature distribution in the standoff region is measured in the presence of a print bed underneath that is maintained at a number of different experiments. These data confirm minimal effect of print bed temperature on measured filament temperature distribution.

As shown in Fig. 2(a) and (b), a FLIR A6703sc InSb infrared camera was positioned at a fixed distance from the nozzle tip to capture temperature distribution along the length of the filament being dispensed. The spatial resolution of these measurements is around 15 μm. Calibration of the IR camera is described next.

### 2.2. Calibration for infrared thermography

While an infrared camera offers a convenient, non-invasive approach for temperature measurement of the entire filament length, careful calibration is needed to ensure accuracy. Experiments are carried out in advance to determine the emissivity of the polymer material and ensure that temperature measurements from the IR camera match well with an independent measurement. For this purpose, a small square sample is printed from the same polymer material that is used for extrusion experiments. This sample is placed on an Instec HCS622V constant temperature stage. Temperature of the top surface of the sample is measured by the infrared camera as well as a T-type thermocouple, monitored through a NI-9213 DAQ thermocouple module and LabView software. Temperature of the thermal stage is varied from room temperature to 230 °C at 20 °C intervals. Once sufficient time has elapsed at each temperature point to reach steady state, temperature of the top surface of the sample is measured by the infrared camera and compared with thermocouple measurements. The experimental setup for calibration is shown in the inset of Fig. 3.

### 2.3. Experiments

Once the various components of the experiment are set up and calibration is completed, a number of experiments are carried out to measure temperature distribution along the filament length up to $x = 1$ mm and understand the effect of various process parameters on the temperature distribution. Filament dispense speed is varied between 2.2 mm/s and 20.2 mm/s by changing the speed of the stepper motor. At each stepper motor setting, the filament dispense speed is determined by measuring the filament length dispensed in a specific time interval. Diameter of the extruded filament is also measured through a micrometer screw gauge. Nozzles of two different diameters – 0.4 mm and 0.6 mm – are used in this work. In order to investigate the effect of convective cooling, air flow at different volumetric flow rates ranging from $12.0 \times 10^{-4}$ m$^3$/s to $22.6 \times 10^{-4}$ m$^3$/s is impinged on the filament from a small fan, which can be seen in the background in Fig. 2(b).

Heat capacity of the filament material – an important parameter for the theoretical model – is measured using a Differential Scanning Calorimeter (DSC) to be 1708 J/kgK. This value is found to vary by less than 3% in the temperature range of 180–215 °C. Further, mass density

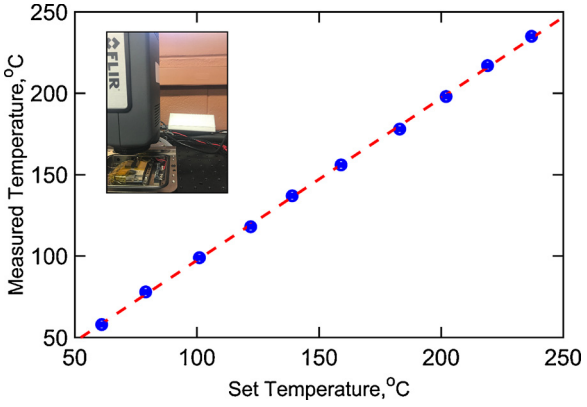


**Fig. 3.** Calibration plot for infrared thermography based on comparison of temperature measured by infrared camera with thermocouple measurement between room temperature and 230 °C. Inset shows a picture of the calibration experiment.

of the extruded material is determined to be 877 kg/m$^3$ by measuring the volume and weight of an extruded filament in a test run.

Key results obtained from these experiments are presented in Section 4.

## 3. Mathematical modeling

A mathematical model is developed for heat transfer in the filament in the standoff region in order to derive an expression for temperature distribution in the filament. Fig. 1(a) shows a schematic of this process. The filament exits the nozzle tip located at $x = 0$ at a temperature $T_0$ with a mass flowrate of $\dot{m}$, and after traveling through the standoff distance, is deposited on the bed at $x = L$. Filament temperature at $x = L$, where the filament reaches the bed is of particular interest. The ambient temperature is assumed to be $T_\infty$. Convective cooling between the filament and ambient is assumed, with a convective heat transfer coefficient $h_c$. Radiative heat transfer may also occur in the standoff region.

Temperature of the print bed under the filament being dispensed is not modeled, because in this case, advective heat transfer along the filament downstream is expected to dominate over thermal diffusion from the print bed into the filament in the standoff region. The ratio of the magnitudes of these two phenomena, called the Peclet number [27] is estimated to be very large, around 200 due to the relatively large value of filament speed and low thermal diffusivity of the filament material. This indicates that the filament temperature distribution in the standoff region is largely unaffected by thermal diffusion from the print bed.

Temperature distribution within the filament, $T(x)$ between $x = 0$ and $x = L$ is assumed to be in steady state. This is expected to be a reasonable assumption beyond the short time during which the filament first leaves the nozzle and travels through the standoff distance. Once filament motion is established within the standoff region, temperature at any location $x$ is expected to be independent of time. The validity of this assumption is confirmed through measurements discussed in Section 4.5. Further, temperature is assumed to vary only in the $x$ direction, and not within the cross-section of the filament. Thermal uniformity in the transverse direction is justified by the very small value of the Biot number in the radial direction [27], estimated to be around 0.02 due to the very small size of the filament. An Eulerian approach is followed in order to determine an expression for $T(x)$. Energy conservation is considered in an infinitesimal element of thickness $dx$ located at distance $x$ from the nozzle tip during steady state, as shown in Fig. 2(b). Thermal energy is advected into this element at the top face along with the extruding filament material, and advected out at the bottom face, as shown in the elemental energy balance schematic in Fig. 2(b). These energy fluxes can be determined through heat capacity of the filament material and the local temperature. In addition, the element loses heat from its peripheral surface area due to convection, radiation or both. Axial thermal conduction effects are neglected due to the large value of the Peclet number. As a result, the overall energy balance for the element is given by

$$\dot{m}C_pT = \dot{m}C_p\left[T + \frac{dT}{dx}dx\right] + h_cP[T-T_\infty]dx + \varepsilon\sigma P(T^4-T_r^4)dx \tag{1}$$

where $P$ is the filament perimeter, assumed not to change along the filament. $C_p$ is the heat capacity of the filament material. $\dot{m}$ is the mass flowrate, given by $\dot{m} = \rho AV$, where ρ is filament density, $A$ is the cross section area and $V$ is the filament speed. $\varepsilon$ and $\sigma$ are the emissivity of the filament and Stefan-Boltzmann constant respectively. $T_r$ is the representative temperature of the surroundings to which the element radiates. $T_r$ is a combination of the temperatures of surfaces in the vicinity of the element, such as the nozzle tip, bed, etc. Eq. (1) can be simplified to

$$\frac{dT}{dx} = -\frac{h_cP}{\dot{m}C_p}(T-T_\infty) - \frac{\varepsilon\sigma P}{\dot{m}C_p}(T^4-T_\infty^4) \tag{2}$$

which is a non-linear ordinary differential equation that governs temperature distribution in the filament. The initial condition at the nozzle tip, $x = 0$ is simply $T = T_0$.

An explicit analytical solution for Eq. (2) is difficult to determine due to the non-linear term. While it can be solved numerically based on the explicit definition of the derivative of temperature in Eq. (2), an analytical solution is sought by linearizing the radiative term in Eq. (2), as is usually done, by writing an approximate radiative heat transfer coefficient, $h_r$ given by [27]

$$h_r = \varepsilon\sigma(T_{eff}^2 + T_r^2)(T_{eff} + T_r) \tag{3}$$

where $T_{eff}$ is the effective filament temperature, which can be approximated with the average filament temperature. Based on this approximation, Eq. (2) can be re-written as

$$\frac{dT}{dx} = -\frac{h_{eff}P}{\dot{m}C_p}(T-T_\infty) \tag{4}$$

where $h_{eff} = h_c + h_r$ is the effective heat transfer coefficient given by the sum of convective and radiative heat transfer coefficients. Based on this simplification, an expression for the temperature distribution in the filament is found to be

$$\theta = \frac{T-T_\infty}{T_0-T_\infty} = exp\left(-\frac{x}{x_0}\right) \tag{5}$$

where the characteristic length $x_0$ is given by

$$x_0 = \frac{\dot{m}C_p}{h_{eff}P} \tag{6}$$

This completes the derivation for the temperature distribution in the filament. Eq. (5) shows that filament temperature reduces exponentially with distance away from the nozzle, and the nature of the exponential decay is governed by the characteristic length $x_0$, which represents the distance by which the temperature has decayed by 1/e = 0.368. Filament temperature at the end of the standoff region can be found by putting $x = L$ in Eq. (5).

The treatment above assumes that thermophysical properties of the filament, such as heat capacity and density do not change appreciably with temperature. This is a reasonable assumption due to the narrow temperature range in a well-designed stand-off gap.

Note that Eq. (5) predicts two very different regimes of the temperature field depending on the value of the characteristic length $x_0$. When $x_0$ is much larger than the standoff distance $L$, Eq. (5) shows that $\theta$ is close to 1, i.e., there is negligible temperature drop in the filament, which reaches the bed at roughly the same temperature as the nozzle tip. In the other extreme, when $x_0 << L$, Eq. (5) shows that $\theta$ is close to 0, i.e., the filament cools down to the ambient temperature, which is undesirable for polymer additive manufacturing. These regimes are investigated further, and $x_0$ is calculated for typical values of the underlying parameters relevant for polymer AM in Section 4.

In general, both convection and radiation may be important heat loss mechanisms. The magnitude of these components can be estimated through an approximate computation of radiative and convective heat fluxes. If under a given set of experimental conditions, radiation is not significant, then Eq. (5) will remain a valid solution with $h_r = 0$. In conditions where radiation is expected to be important, either Eq. (2) can be solved numerically, or, as an approximation, the radiative heat transfer coefficient $h_r$ can be computed from Eq. (3), so that the solution is given by Eq. (5), with $h_{eff} = h_c + h_r$. In general, modeling of radiative heat transfer is quite complicated, particularly in this case, due to the presence of a surface hotter than the filament (nozzle) as well as one that is cooler than the filament (platform bed).

## 4. Results and discussion

### 4.1. Infrared thermography calibration

Temperature of a small part printed with the same filament material used in this work is measured by the infrared camera at a number of different temperatures following the procedure discussed in Section 2. Fig. 3 plots the temperature measured by the infrared camera against the temperature measured by a thermocouple located next to the point of infrared temperature measurement, while the entire setup is mounted on a temperature-controlled stage. Fig. 3 shows that over the entire measurement range, temperature measured through infrared thermography is close to the temperature measured by the thermocouple. All measurement points lie very close to the ideal 45° line on which the infrared measured temperature is equal to the set temperature. This establishes the accuracy of the infrared based temperature measurement method. The emissivity of the filament material is determined to be 0.92 through this calibration and used throughout this work.

### 4.2. Filament temperature measurement and comparison with analytical model

Infrared thermography enables non-invasive measurement of temperature distribution along the entire standoff region simultaneously. This is carried out for a number of different process parameters in order to understand the effect of these parameters on the temperature distribution and to compare against the analytical model.

In the first set of experiments, the filament temperature distribution is measured at five different filament speeds. Measurements are carried out for 0.4 mm and 0.6 mm nozzle diameters, which are most commonly used for polymer-based additive manufacturing. The nozzle temperature is maintained at 215 °C. No active cooling is provided, as is typical of polymer AM processes. Fig. 4(a) and (b) summarize these data by plotting the measured filament temperature as a function of $x$ for multiple filament speeds for 0.4 mm and 0.6 mm diameter nozzles respectively. The filament speeds listed in these Figures are different for different diameter nozzles. These are values measured for five specific motor speeds in the experimental setup. In each case, filament temperature drops as $x$ increases, which is expected due to increased convective heat loss along the filament length. Further, filament temperature also reduces as the filament speed goes down, which is also expected due to the reduced advection of thermal energy at lower filament speeds.

Fig. 4(a) and (b) also plot the temperature distribution predicted by the analytical model given by Eq. (5). There is very good agreement between the experimental data and analytical model over a broad range of parameters. For each nozzle, as the filament speed increases, there is greater amount of heat advected into any point in the filament in the standoff region, resulting in lower and lower temperature drop in the standoff region. This is the desired regime of operation for a polymer AM process that corresponds to a large value of the characteristic length $x_0$. Note that the heat transfer coefficients for the theoretical model plots in Fig. 4 are in the 20–40 W/m$^2$K range. This is somewhat greater than values for free convection heat transfer [27] because of two possible reasons. Firstly, the downwards motion of the filament in the stand-off region relative to the ambient air may result in some air flow, and hence, enhanced convection heat transfer. Secondly, the measured heat transfer coefficient includes contributions from radiative heat transfer, which may also raise the value of the heat transfer coefficient above what may be expected for free convection alone.

Note that the perimeter $P$ in Eq. (5) for the analytical model curves in Fig. 4 is computed based on the actual diameter of the extruded filament, and not the nozzle diameter, due to the well-known phenomenon of polymer swelling in nozzle based extrusion [28]. The perimeter is assumed to stay constant throughout the standoff region, which is verified through measurement of the diameter of the extruded filament at a number of axial locations.

Further, note that in Fig. 4 as well as subsequent figures, temperature is plotted in the non-dimensional form as given by Eq. (5). This ensures consistency of results for different values of nozzle and ambient temperatures. As an example, for nozzle and ambient temperatures of 200 °C and 25 °C respectively, a range of 0.05 on the $y$ axis in Fig. 4 corresponds to a temperature drop of 8.75 °C.

The effect of active cooling of the filament during extrusion is considered next. A set of experiments is carried out where the filament is cooled with impinging air flow from a fan at different speeds. As the air speed increases, greater convective heat transfer, and therefore, a greater value of $h_c$ is expected. This is expected to push the filament into the small $x_0$ regime, where convective heat loss dominates and results in significant temperature drop across the standoff region. Fig. 5(a) and (b) plot temperature as a function of $x$ for a number of cooling conditions at two different filament speeds for a 0.4 mm diameter nozzle. Similar data are plotted for a 0.6 mm diameter nozzle in Fig. 6(a) and (b). Data show, as expected, greater temperature drop as more and more cooling is provided. There is good agreement between experimental data and the predicted thermal behavior based on the theoretical model. In Fig. 5(b), experimental data and model for the two forced cooling cases are very close to each other, which is likely because the high filament speed in this case results in reduced sensitivity on flow speed for forced convection cooling. Clearly, as shown in Figs. 5 and 6, active cooling of the filament in the standoff region is undesirable, as it leads to reduced filament temperature when it reaches the bed. Some cooling, however, is always expected even in the absence of forced air flow due to free convection heat transfer and possibly due to radiation.

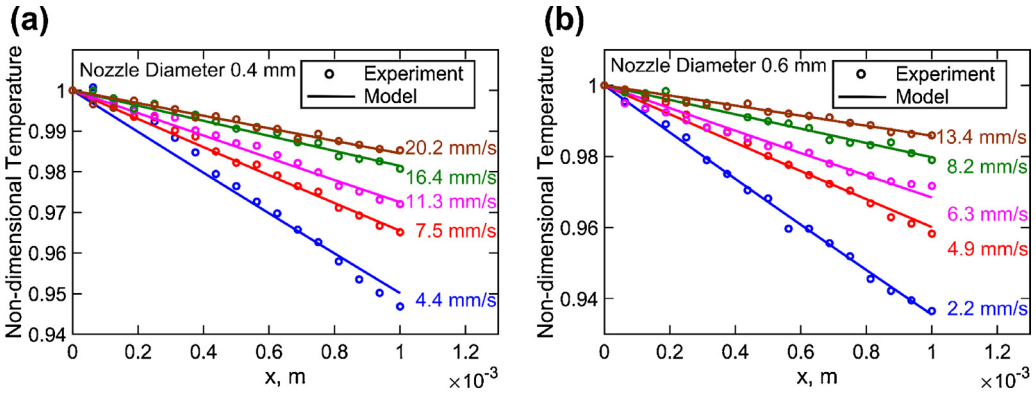


**Fig. 4.** Comparison of measured temperature distribution in the standoff region as a function of $x$ with prediction from theoretical model for multiple filament speeds. (a)-(b) present this comparison for 0.4 mm and 0.6 mm nozzle diameters respectively.

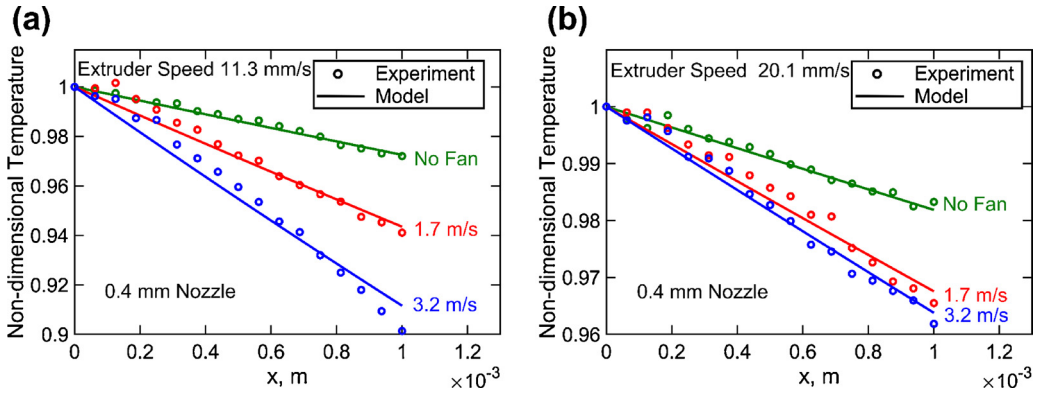


**Fig. 5.** Comparison of measured temperature distribution in the standoff region as a function of $x$ with prediction from theoretical model for three different cooling conditions. (a) and (b) present this comparison for two different filament speeds respectively. The nozzle diameter is 0.4 mm in both cases.

Finally, experiments are carried out for studying the effect of the nozzle diameter on thermal characteristics of the filament in the standoff region. Nozzles of two different outlet diameters are used to dispense the filament at two different motor speeds, and temperature field is measured in each case. Fig. 7 presents these experimental measurements as a function of $x$, as well as the corresponding analytical model curves. Similar to previous figures, there is very good agreement between experimental data and analytical model for a number of nozzle diameters. As the nozzle diameter increases, Fig. 7 shows lower reduction in temperature at a larger nozzle diameter, which occurs due to increased advection of heat along with the dispensed filament. This is consistent with the definition of the characteristic length in Eq. (6), which shows that for the same filament speed, characteristic length increases with increasing nozzle diameter, thereby resulting in reduced temperature drop across the standoff region. This Figure also shows that the larger the filament speed, the lower is the temperature drop, which is again consistent with the theoretical result. Note that an advantage of a larger nozzle is the reduced pumping work needed to push the filament through the nozzle.

Figs. 4–7 demonstrate quantitative agreement between experimental data and the analytical model derived in Section 2. This validates the analytical model, and establishes it as a useful tool for thermal design of the extrusion process. As shown in these measurements, the desired effect of minimum temperature drop in the standoff region can be achieved by a combination of large mass flowrate, large heat capacity and minimum convective cooling. Some of these requirements present trade-offs and challenges with respect to other considerations. For example, a large mass flowrate through a small nozzle requires very large pressure in the nozzle assembly. Reduced filament diameter may also affect throughput because the extruder will need to make more passes to cover the same area, although, it may improve spatial resolution of the print.

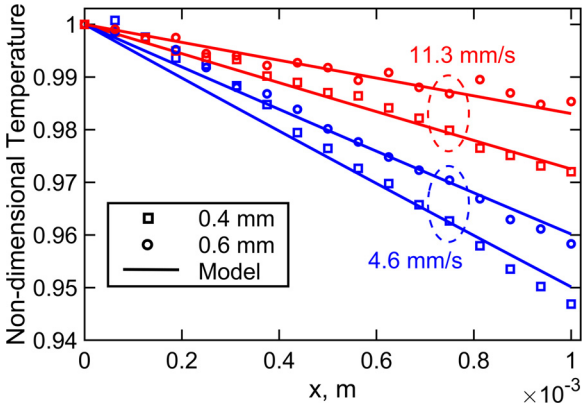


**Fig. 7.** Comparison of measured temperature distribution in the standoff region as a function of $x$ with prediction from theoretical model for two different nozzle diameters.

### 4.3. Thermal regimes based on characteristic length

Eq. (5) shows that the temperature in the filament decays exponentially as distance from the nozzle tip increases. Specifically, filament temperature at the end of the standoff region, $x = L$, a key parameter that ultimately affects bond quality between adjacent filaments is given by

$$\theta_L = \frac{T(L) - T_\infty}{T_0 - T_\infty} = exp\left(-\frac{L}{x_0}\right) \tag{7}$$

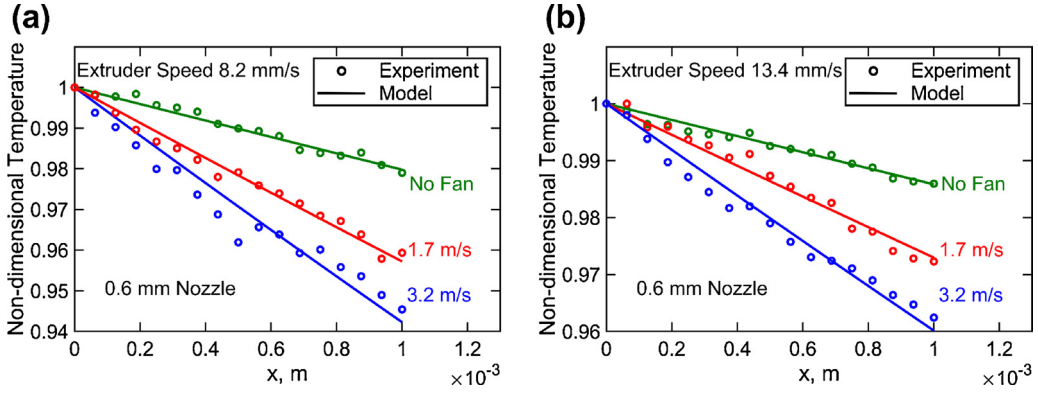


**Fig. 6.** Comparison of measured temperature distribution in the standoff region as a function of $x$ with prediction from theoretical model for three different cooling conditions. (a) and (b) present this comparison for two different filament speeds respectively. The nozzle diameter is 0.6 mm in both cases.

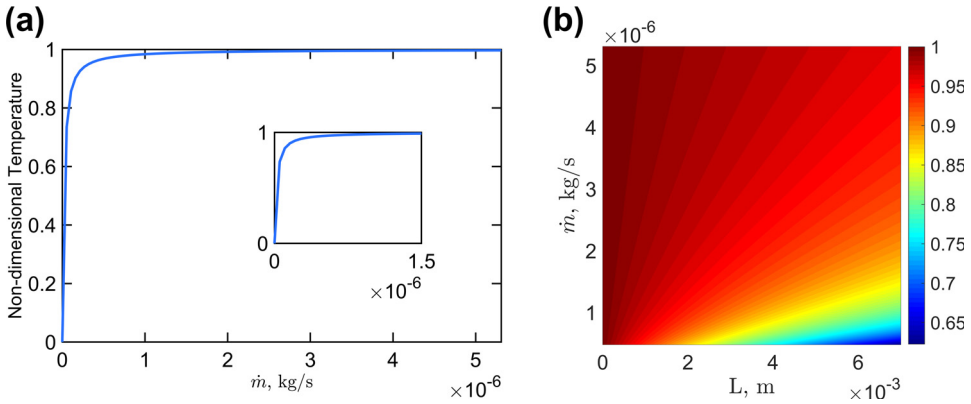


**Fig. 8.** (a) Theoretically predicted temperature at the end of the standoff region as a function of mass flowrate, with all other parameters held constant. (b) Colormap showing the variation of theoretically predicted temperature at the end of the standoff region as a function of standoff distance and mass flowrate.

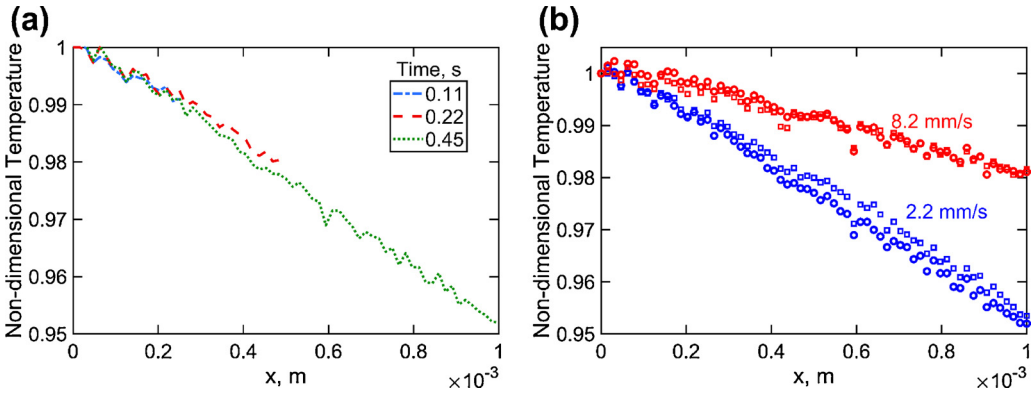


**Fig. 9.** Validation of steady state assumption: (a) Measured filament temperature in the standoff region as a function of $x$ at four different times. (b) Filament temperature in the standoff region as a function of $x$ measured at two different times (shown as circles and squares)for two different speeds.

The characteristic length, $x_0$, given by Eq. (6) is a key parameter that governs the temperature distribution. $x_0$ represents the balance between two processes – heat advection due to material flow and heat loss from the periphery of the filament. Based on the value of $x_0$ relative to $L$, there exist two distinct regimes with very different nature of temperature decay. When $x_0/L$ is very large, heat advection is much larger than heat loss, due to the dominance of mass flowrate and heat capacity over convective/radiative heat transfer coefficient and perimeter. In this regime, sufficiently large amount of heat continues to enter into the filament region, due to which, the temperature of the filament does not decay much through the filament length. This is also seen mathematically from Eq. (7) that shows that $\theta_L$ tends to 1 when $x_0/L$ is large. This regime can be interpreted as being an advection-dominated regime. On the other hand, when $x_0/L$ is small, there is relatively greater rate of heat loss than advection, and therefore, most of the filament cools down to the ambient temperature. The low $x_0$ regime is convection-dominated, wherein Eq. (7) shows that $\theta_L$ tends to 0 when $x_0/L$ is small.

Clearly, an effective dispensing process for additive manufacturing must be in the advection-dominated, large $x_0/L$ regime, which can be ensured through a large filament mass flowrate, large heat capacity filament material and low rate of cooling. By doing so, it can be ensured that the filament is dispensed on the bed at about the same temperature as the nozzle tip. Some of these considerations may present significant challenges in the operation of the nozzle assembly.

For any practical polymer additive manufacturing process, Eq. (6) can be used to determine the value of $x_0$ and therefore determine which regime the process lies in. As an illustration, for a 0.6 mm diameter nozzle extruding ABS ($\rho = 877$ kg/m$^3$, $C_p = 1708$ J/kgK) at 20 mm/s with $h_{eff} = 31$ W/m$^2$K, $x_0$ is found to be 0.14 m, which is at least two orders of magnitude larger than typical standoff distance (less than 1 mm). This indicates that heat transfer in the standoff region in a typical polymer printing process is advection dominated. Assuming nozzle tip temperature of 200 °C, ambient temperature of 25 °C and a standoff distance of 0.5 mm, temperature at the end of the standoff region is found to be 199.4 °C, indicating negligible temperature drop in the standoff region under this set of parameters. If the nozzle diameter is changed to 0.1 mm at the same filament speed, $x_0$ is now found to be 0.024 m, resulting in a lower temperature of 196.4 °C at the end of the standoff region due to reduced dominance of advection. Note that these parameters have been chosen as an illustration. These parameters can vary over a broad range of polymer AM processes, and the model is capable of thermally characterizing the process, given the values of these parameters.

### 4.4. Design space exploration with analytical model

The analytical heat transfer model presented in Section 2, and validated through experimental measurements can be used for design space exploration. Specifically, the range of various process parameters that ensure the thermal objective of minimum temperature drop in the standoff region can be determined based on the experimentally validated model. Fig. 8(a) plots temperature at the end of the standoff region as a function of mass flowrate. The standoff region is assumed to be 0.5 mm long. 0.4 mm diameter nozzle is assumed. Heat transfer coefficient is taken to be 31 W/m$^2$K. Fig. 8(a) shows that temperature drop across the standoff region decreases as the extruder speed goes up. There is a certain threshold value of the mass flowrate that will meet a given specification of the maximum acceptable temperature drop. Beyond that threshold, any filament mass flowrate is thermally

acceptable. This mass flowrate threshold shown in Fig. 8(a) is rather small, and is likely to be met by any reasonably designed polymer AM process.

The standoff distance itself is an important design variable, which is usually chosen to be a small value. Fig. 8(b) presents a colormap of temperature at the end of the standoff region as a function of ABS filament mass flowrate $\dot{m}$ and standoff distance $L$. Nozzle diameter of 0.4 mm and heat transfer coefficient of 31 $W/m^2K$ are assumed. Fig. 8(b) shows that the computed temperature depends on both variables. There is a distinct region of large $\dot{m}$ and small $L$ where the temperature is very close to the nozzle tip temperature ($\theta_L$ close to 1). On the other hand, when mass flowrate is relatively small and the standoff distance is relatively large, there is significant temperature drop in the standoff region ($\theta_L$ much less than 1). Fig. 8(b) shows that a large standoff distance can be compensated somewhat by increasing the mass flowrate in order to meet the same thermal objective of a fixed temperature drop in the standoff region.

Design curves such as Fig. 8(a) and (b) demonstrate the capability of the experimentally validated analytical model presented here for accurate thermal analysis of the process. This could be used for understanding and operating the process in a parameter space that ensures good thermal performance. These design curves can also be used for understanding and optimizing trade-offs between thermal performance and other system-level objectives.

### 4.5. Validation of steady assumption

A key assumption made in the theoretical analysis presented in section 2 is that the filament temperature field in the standoff region remains steady. This is analogous to the steady state assumption commonly made in internal fluid flow analysis. In order to validate this assumption, the filament temperature field is measured at multiple times while the filament continues to be dispensed. Filament temperature is plotted as a function of the axial coordinate, $x$, for multiple times in Fig. 9(a), showing that while the filament temperature changes with $x$, there is no appreciable change in the filament temperature field. For further validation of the assumption of steady temperature, the filament temperature is measured as a function of $x$ at multiple times for two different filament speeds. These data, plotted in Fig. 9(b) show that at both speeds, the temperature vs. $x$ plot remains invariant with time. This further confirms a key assumption underlying the theoretical model.

## 5. Conclusions

This paper investigates an important and previously unaddressed heat transfer process in polymer extrusion based additive manufacturing processes through both experimental measurements and analytical modeling. Heat transfer processes in the standoff region play a key role in determining the filament temperature as it reaches the bed. Results from this work help identify the key process and material parameters that affect heat transfer in the standoff region. Two distinct regimes of heat transfer in the standoff region are identified based on the value of a single parameter named the characteristic length that combines mass flowrate, heat capacity, filament size and cooling conditions. The good agreement of the analytical model with experimental data is encouraging. Results presented here may help develop practical design tools to improve thermal performance as well as address trade-offs between heat transfer and other performance parameters of extrusion based polymer additive manufacturing.

## Acknowledgment

The authors would like to acknowledge assistance from Mr. Amirhossein Mostafavi and Mr. Santnam Bakshi in heat capacity measurements.

## References

[1] D. Dimitrov, K. Schreve, N. de Beer, Advances in three dimensional printing – state of the art and future perspectives, Rapid Prototyping J. 12 (2006) 136–147.
[2] D.T. Pham, R.S. Gault, A comparison of rapid prototyping technologies, Int. J. Mach. Tools Manuf. 38 (1998) 1257–1287.
[3] K.V. Wong, A. Hernandez, A review of additive manufacturing, ISRN Mech. Eng. (2012) 1–10 208760.
[4] J.P. Kruth, M.C. Leu, T. Nakagawa, Progress in additive manufacturing and rapid prototyping, CIRP Ann. Manuf. Technol. 2 (1998) 525–540.
[5] P. Vojislav, V.H.G. Juan, J.F. Olga, D.G. Javier, R.B.P. Jose, P.G. Luis, Additive layered manufacturing: sectors of industrial application shown through case studies, Int. J. Mech. Prod. Eng. Res. Dev. 49 (2010) 1061–1079.
[6] I. Campbell, D. Bourell, I. Gibson, Additive manufacturing: rapid prototyping comes of age, Rapid Prototyping J. 18 (2012) 255–258.
[7] I. Zein, D.W. Hutmacher, K.C. Tan, S.H. Teoh, Fused deposition modeling of novel scaffold architectures for tissue engineering applications, Biomaterials 4 (2000) 1169–1185.
[8] D. Ravoori, L. Alba, H. Prajapati, Investigation of Process-Structure-Property Relationships in Polymer Extrusion Based Additive Manufacturing Through In Situ High Speed Imaging and Thermal Conductivity Measurements, Addit. Manuf. 23 (2018) 132–139, https://doi.org/10.1016/j.addma.2018.07.011.
[9] Q. Sun, G.M. Rizvi, C.T. Bellehumeur, P. Gu, Effect of processing conditions on the bonding quality of FDM polymer filaments, J. Manufac. Process 14 (2008) 72–80.
[11] H. Prajapati, D. Ravoori, R.L. Woods, A. Jain, Measurement of anisotropic thermal conductivity and inter-layer thermal contact resistance in polymer fused deposition modeling (FDM), Addit. Manuf. 21 (2018) 84–90, https://doi.org/10.1016/j.addma.2018.02.019.
[10] S.F. Costa, F.M. Duarte, J.A. Covas, Estimation of filament temperature and adhesion development in fused deposition techniques, J. Mater. Process. Technol. 245 (2017) 167–179.
[12] M.A. Yardimci, S. Güçeri, Conceptual framework for the thermal process modelling of fused deposition, Rapid Prototyping J. 2 (1996) 26–31.
[13] J.H. Park, M.Y. Lyu, S.Y. Kwon, H.J. Roh, M.S. Koo, S.H. Cho, Temperature analysis of nozzle in a FDM type 3D printer through computer simulation and experiment, Elastomers Compos. 51 (2016) 301–307.
[14] F. Peng, B.D. Vogt, M. Cakmak, Complex flow and temperature history during melt extrusion in material extrusion additive manufacturing, Addit. Manuf. 22 (2018) 197–206.
[15] C.T. Bellehumeur, L. Li, Q. Sun, P. Gu, Modeling of bond formation between polymer filaments in the fused deposition modeling process, J. Manuf. Process 06 (2004).
[16] M.E. Mackay, Z.R. Swain, C.R. Banbury, The performance of the hot end in a plasticating 3D printer, J. Rheol. 61 (2017) 229–236.
[17] J. Go, S.N. Schiffres, A.G. Stevens, A.J. Hart, Rate limits of additive manufacturing by fused filament fabrication and guidelines for high-throughput system design, Addit. Manuf. 16 (2017) 1–11.
[18] E.L. Gilmer, D. Miller, C.A. Chatham, C. Zawaski, J.J. Fallon, A. Pekkanen, T.E. Long, C.B. Williams, M.J. Bortner, Model analysis of feedstock behavior in fused filament fabrication: enabling rapid materials screening, Polymer 152 (2017) 51–61, https://doi.org/10.1016/j.polymer.2017.11.068.
[19] A. Bellini, S. Guceri, M. Bertoldi, Liquefier dynamics in fused deposition, J. Manuf. Sci. Eng. 126 (2004) 237–246.
[20] J. Go, A.J. Hart, Fast desktop-scale extrusion additive manufacturing, Addit. Manuf. 18 (2017) 276–284.
[21] D.D. Phan, Z.R. Swain, M.E. Mackay, Rheological and heat transfer effects in fused filament fabrication, J. Rheol. 62 (2018) 1097–1107.
[22] F. Penga, B.D. Vogta, M. Cakmak, Complex flow and temperature history during melt extrusion in material extrusion additive manufacturing, Rapid Prototyping J. 22 (2018) 197–206.
[23] J.E. Seppala, K.D. Migler, Infrared thermography of welding zones produced by polymer extrusion additive manufacturing, Addit. Manuf. 12 (2016) 71–76.
[24] H. Xia, J. Lu, S. Dabiri, G. Tryggvason, Fully resolved numerical simulations of fused deposition modeling. Part I: fluid flow, Rapid Prototyping J. 24 (2018) 463–476.
[25] A. D'Amico, A. Peterson, An adaptable FEA simulation of material extrusion additive manufacturing heat transfer in 3D, Addit. Manuf. 21 (2018) 422–430.
[26] A. Bendada, M. Lamontagne, A new infrared pyrometer for polymer temperature measurement during extrusion moulding, Infrared Phys. Technol. 46 (2004) 1–15.
[27] F.P. Incropera, D.P. DeWitt, T.L. Bergman, A.S. Levine, Introduction to Heat Transfer, 5th ed., John Wiley & Sons, 2006.
[28] R.I. Tanner, A theory of die-swell revisited, J. Non-Newton. Fluid Mech. 129 (2005) 85–87.